

ADformer: A Multi-Granularity Spatial-Temporal Transformer for EEG-Based Alzheimer Detection

Yihe Wang, Nadia Mammone, Darina Petrovsky,
Alexandros T. Tzallas, Francesco C. Morabito, Xiang Zhang

Abstract— **Electroencephalography (EEG) has emerged as a cost-effective and efficient tool to support neurologists in the detection of Alzheimer’s Disease (AD). However, most existing approaches rely heavily on manual feature engineering or data transformation. While such techniques may provide benefits when working with small-scale datasets, they often lead to information loss and distortion when applied to large-scale data, ultimately limiting model performance. Moreover, the limited subject scale and demographic diversity of datasets used in prior studies hinder comprehensive evaluation of model robustness and generalizability, thus restricting their applicability in real-world clinical settings.** To address these challenges, we propose **ADformer**, a novel multi-granularity spatial-temporal transformer designed to capture both temporal and spatial features from raw EEG signals, enabling effective end-to-end representation learning. Our model introduces multi-granularity embedding strategies across both spatial and temporal dimensions, leveraging a two-stage intra–inter granularity self-attention mechanism to learn both local patterns within each granularity and global dependencies across granularities. We evaluate **ADformer** on 4 large-scale datasets comprising a total of 1,713 subjects, representing one of the largest corpora for EEG-based AD detection to date, under a cross-validated, subject-independent setting. Experimental results demonstrate that **ADformer** consistently outperforms existing methods, achieving subject-level F1 scores of 92.82%, 89.83%, 67.99%, and 83.98% on the 4 datasets, respectively, in distinguishing AD from healthy control (HC) subjects.

Index Terms— Alzheimer’s Disease, Dementia, EEG, Time Series, Transformers, Deep Learning

I. INTRODUCTION

Alzheimer’s disease (AD) is the most prevalent neurodegenerative disorder among the elderly population worldwide [1], affecting an estimated 10-30% of individuals over the age of 65, with an annual incidence rate of 1-3% [2]. AD is characterized by the accumulation of amyloid- β peptides in the brain due to impaired clearance mechanisms [3].

Yihe Wang and Xiang Zhang are with the Department of Computer Science, University of North Carolina - Charlotte, Charlotte, North Carolina 28223, United States.

Nadia Mammone and Francesco C. Morabito are with the DICEAM Department, University Mediterranea of Reggio Calabria Via Zehender, Feo di Vito, 89122 Reggio Calabria, Italy.

Darina Petrovsky is with the School of Nursing, Duke University, Durham, North Carolina 27708, United States.

Alexandros T. Tzallas is with the Department of Informatics & Telecommunications, University of Ioannina, Kostakioi, GR-47100, Arta, Greece.

Xiang Zhang is the corresponding author (E-mail: xiang.zhang@charlotte.edu). The code is available at <https://github.com/DL4mHealth/ADformer>

Clinically, the disease progresses in stages, typically advancing from healthy aging to mild cognitive impairment (MCI) and ultimately to overt AD. Although a definitive cure for AD remains elusive, early detection and intervention have been shown to temporarily slow symptom progression and improve patients’ quality of life [4], [5]. Current diagnostic tools for AD primarily rely on neuroimaging techniques such as Magnetic Resonance Imaging (MRI) and Positron Emission Tomography (PET) [6], [7]. However, these methods are costly, require specialized medical infrastructure and expertise, and are often applied only after significant cognitive impairment has occurred. Electroencephalography (EEG) has recently emerged as a promising alternative for the early and timely detection of AD. EEG offers several advantages, including non-invasive, real-time monitoring, affordability, and portability, making it particularly suitable for widespread clinical use [8], [9]. Effective AD detection using EEG may also enable integration with mobile health platforms, supporting both home-based early detection and continuous tracking of disease progression.

Over the past two decades, research on EEG-based AD detection has primarily followed two main directions for interpreting EEG signals. The first approach relies on handcrafted biomarker extraction, where features such as statistical [10], [11], spectral [12], [13], power [14], [15], and complexity-based [16], [17] metrics are used. These features are then used as input to conventional machine learning classifiers, such as multi-layer perceptrons (MLPs) and support vector machines (SVMs), for final prediction. The second direction leverages modern deep learning techniques applied to 1D EEG signals or their transformed representations. Commonly used architectures include convolutional neural networks (CNNs) [9], [18], [19], graph convolutional networks (GNNs) [20], [21], and transformers [22], which have demonstrated superior performance by learning spatial-temporal features.

However, existing methods for EEG-based AD detection suffer from two major limitations. First, most approaches still rely on manual feature engineering or data transformation, lacking a truly end-to-end learning framework, whether traditional machine learning or deep learning is used. For instance, some studies convert 1D EEG signals into time-frequency representations using techniques such as the Short-Time Fourier Transform (STFT) [23] or the Continuous Wavelet Transform (CWT) [24], and subsequently apply 2D CNNs for feature extraction on the resulting spectrogram images. While these transformations may facilitate feature learning by highlighting certain signal properties, they often distort or

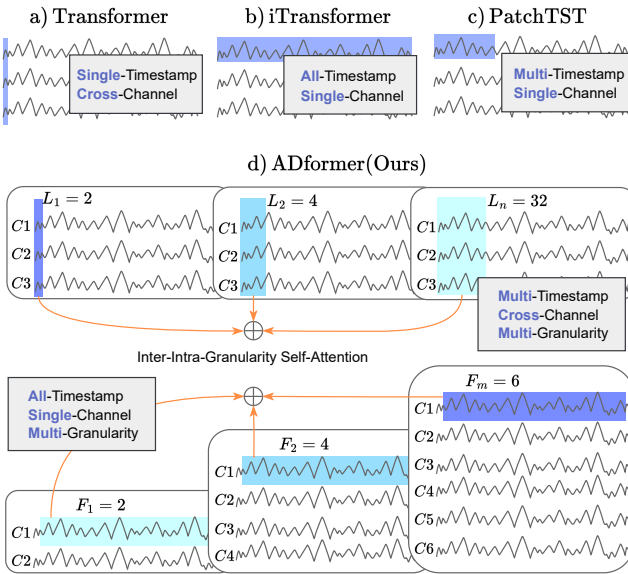


Fig. 1: Token embedding methods. Vanilla Transformer, Autoformer, and Informer [26]–[28] employ a single cross-channel timestamp as a token, while iTransformer [29] utilizes the whole series of a single channel as a token. PatchTST and Crossformer [30], [31] adopt a patch of timestamps from a single channel as a token. For ADformer, we propose one method that repetitively segments input into patches of varying lengths, each defined as one granularity, and embeds these cross-channel patches. Another method repetitively adjusts the number of channels in EEG data using 1-D convolutions, each specific target channel number defined as one granularity, and embeds the whole series of each channel.

discard raw signal information, potentially eliminating valuable patterns in the temporal, frequency, or spatial domains. Second, due to the limited availability and high cost of collecting EEG-based AD datasets, many existing studies are conducted on relatively small cohorts—typically involving 20 to fewer than 200 subjects [25]—and are usually restricted to a single dataset. This lack of subject scale and demographic diversity hinders the comprehensive evaluation of model robustness and generalizability, thereby limiting the clinical applicability of these methods in real-world settings.

To bridge these gaps, we propose an end-to-end multi-granularity spatial-temporal transformer, named **ADformer**. Our method operates directly on 1D EEG signals, eliminating the need for manual feature extraction or data transformation. A preliminary version of this work, **Medformer**, was introduced in [32]. It employs cross-channel multi-granularity patch embedding and intra-inter-granularity self-attention to jointly capture spatial and temporal dependencies, and was evaluated on various tasks of medical time series classification, including EEG and ECG. In this paper, we extend and adapt the Medformer architecture to suit EEG signals better and focus specifically on the task of EEG-based Alzheimer’s Disease (AD) detection. Given the richer spatial information inherent in EEG signals compared to other medical time series, we introduce an additional branch to model spatial features more explicitly. Specifically, we scale up the raw EEG channel

into different numbers depending on varying granularities and embed the entire series from each channel as a whole-series multi-granularity channel embedding. We designate the original cross-channel multi-granularity patch embedding as the **temporal branch**, and the newly proposed whole-series multi-granularity channel embedding as the **spatial branch**. Figure 1 provides a comparative overview of our data embedding strategy versus existing approaches used in time series transformers [26], [29], [30]. The embeddings from both branches are processed independently through intra-inter-granularity self-attention modules, enabling the model to capture local dependencies within each granularity and global interactions across granularities. We evaluate ADformer on four large-scale datasets comprising a total of 1,713 subjects and 2,595,150 one-second EEG samples, forming one of the most comprehensive EEG-based AD detection corpora to date. Our approach is compared against 8 baselines, including 1 traditional manual feature extraction method and 7 state-of-the-art (SOTA) deep learning models. We conduct extensive experiments under two classification settings: (1) multi-class classification across various brain disorders, and (2) binary classification tasks between AD and HC subjects, both using a rigorously designed **subject-independent** cross-validation protocol. We further investigate additional factors such as the impact of sample length and overlapping rate for detection performance. Our method achieves the best performance in 24 out of 32 metrics across the four datasets and two classification settings. Notably, ADformer achieves the best subject-level performance across all datasets, demonstrating strong real-world applicability. Specifically, the subject-level F1 scores for distinguishing AD from healthy controls are 92.82%, 89.83%, 67.99%, and 83.98%, respectively.

We summarize our key contributions as follows:

- 1) We introduce ADformer, a novel end-to-end multi-granularity spatial-temporal transformer designed explicitly for EEG-based Alzheimer’s disease (AD) detection.
- 2) We conduct comprehensive experiments on 4 large-scale EEG datasets, with a total of 1,713 subjects and 2,595,150 1-second samples, forming the world’s largest corpora to date in EEG-based AD detection, to demonstrate the generalization capability of our model.
- 3) We compare ADformer with 1 handcrafted feature-based method and 7 SOTA deep learning methods—evaluations including multi-class and AD vs HC classification tasks, both under the cross-validated subject-independent setting. The influence of sample length and overlapping rate on detection performance is also explored.

The rest of the paper is organized as follows: Section II reviews related works, including existing methods for EEG-based AD analysis and transformers in EEG. Section III discusses preliminaries of experimental setups and their significance and defines the research problem. In Section IV, we detail the architecture of the proposed method. Section V provides information on the datasets used and implementation details. Section VI presents the results and their analysis for our method and all baselines under different experimental setups. Finally, we conclude the paper and suggest future works in Section VII.

II. RELATED WORK

A. EEG-based Alzheimer's Disease Detection

In EEG-based analysis for Alzheimer's Disease (AD), two primary research directions have emerged: manual feature extraction and deep learning. **Manual Feature Extraction.** This approach involves identifying handcrafted features—such as entropy, band power, and spectral characteristics—followed by applying conventional classifiers like Multi-Layer Perceptron (MLP) or Support Vector Machine (SVM). Commonly used statistical features include mean, skewness, kurtosis, standard deviation, max, min, and median [10], [11], [33]–[37]. Spectral features encompass phase shift, phase coherence, bispectrum, bicoherence, spectral centroid, spectral roll-off, spectral peak, average magnitude, median frequency, and amplitude modulation [12], [13], [38]–[42]. Power features include power spectral density, relative band power, EEG rhythm ratios, and energy [14], [15], [34], [43], while complexity features comprise various entropy measures such as Shannon entropy, Tsallis entropy, and spectral entropy [16], [17], [44]. The primary advantage of this approach is its interpretability, which makes it more accessible for clinical application. **Deep Learning.** In contrast, deep learning approaches automatically extract features from data and have demonstrated strong performance, particularly on large-scale datasets. A common strategy is to convert EEG signals into image-like representations to capture frequency- or energy-related characteristics. Examples include computing power spectral density (PSD) across channels [9], generating 2D representations of EEG sub-bands (e.g., theta, alpha, beta) [45], and transforming EEG signals into time–frequency (TF) images using the Short-Time Fourier Transform (STFT) for 2D CNN classification [19]. Beyond frequency-based representations, some methods incorporate spatial–temporal structure. For instance, spatial–temporal graph convolutional networks (GCNs) leverage the topological structure of EEG connectivity and dynamic temporal information [20], while gated GCNs enhance node features with PSD similarity for adaptive graph learning [21]. Transformer-based models have also been explored, such as DICE-Net, which combines PSD and Wavelet transforms with a 2D CNN and self-attention module [22]. However, most existing deep learning methods rely on transforming 1D EEG signals into 2D representations (e.g., images or graphs). Fully end-to-end approaches that operate directly on raw 1D EEG data remain underexplored.

B. Transformer for EEG

End-to-end transformers have demonstrated promising results in the EEG domain across a variety of tasks. For example, the work in [46] leverages spatial–temporal information for transformer-based feature embedding in motor imagery classification. EEG-Conformer [47] incorporates both temporal and spatial convolutions for token embedding, and has shown effectiveness on motor imagery and emotion recognition tasks. Other models, such as BIOT [48] and Medformer [32], extend transformer architectures to handle diverse biomedical signals, including EEG. These models utilize either single-channel or cross-channel patching strategies for token embedding, demonstrating strong performance across modalities. More

recently, end-to-end transformers have been explored as backbone architectures for pretraining EEG foundation models. For instance, LabraM [49], EEGPT [50], and EEGformer [51] apply techniques such as vector quantization, momentum alignment, and masked-reconstruction self-supervised on single-channel transformer patches. CBraMod [52] integrates time–frequency patch embeddings with a two-stage transformer that separately captures temporal and spatial representations. These existing studies highlight the potential of end-to-end transformers for EEG classification, especially in terms of scalability and representation learning. This motivates further exploration of end-to-end transformer architectures for EEG-based AD detection, a domain where such methods remain underexplored.

III. PRELIMINARIES AND PROBLEM DEFINITION

A. EEG-Based Disease Detection

In EEG data collected for disease detection tasks, each subject is typically assigned a single label indicating their brain health status, such as the presence or absence of specific neurological conditions. In some cases, multiple labels may be assigned to a subject if they exhibit comorbid neurological conditions, as many brain diseases are not mutually exclusive [53]. To improve memory and computational efficiency in deep learning models, long EEG recordings (e.g., trials or sessions) are commonly segmented into shorter samples. As a result, each EEG sample is generally associated with a disease label and a subject ID indicating the subject's belonging. Since the ultimate goal is to determine whether a subject has a particular disease, post-processing techniques are often employed to aggregate predictions across all samples from the same subject. A widely used approach is majority voting, where the subject is assigned the label that appears most frequently among their samples [9].

B. Subject-Independent Evaluation

In EEG-based brain disease detection, subject-specific features can significantly influence model performance. As a result, different experimental setups may yield vastly different outcomes, potentially leading to misleading conclusions [54]. Therefore, experimental protocols must be carefully designed to align with real-world clinical applications. In the context of EEG-based AD detection, two commonly used evaluation setups exist: subject-dependent [55], [56] and subject-independent [57], [58]. In subject-dependent setups, samples from all subjects are randomly shuffled and then split into training, validation, and test sets. As a result, data from the same subject may appear in multiple sets, potentially causing information leakage and overestimating model performance. In contrast, subject-independent setups divide the data strictly by subject, ensuring that samples from the same subject are present in only one of the three subsets—training, validation, or testing. Figure 2, adopted from [59], provides a simple illustration of these two setups. In this work, we adopt the subject-independent setup, as it better simulates real-world deployment scenarios on unseen subjects and prevents information leakage arising from subject-specific features during training.

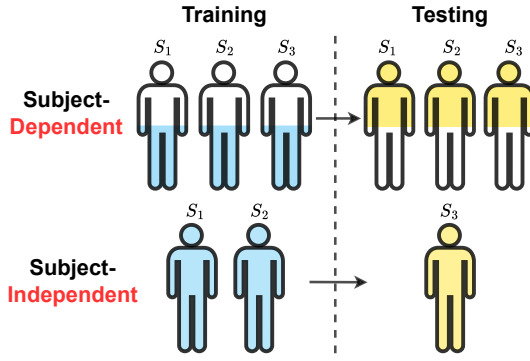


Fig. 2: Subject-dependent/independent setups. In the subject-dependent setup, samples from the same subject can appear in both the training and test sets, causing information leakage. In the subject-independent setup, samples from the same subject are exclusively in either the training or test set, which is more challenging and practically meaningful but less studied.

C. Problem Definition

EEG-based Alzheimer’s Disease (AD) Detection. Let the input EEG sample be denoted as $x_{\text{in}} \in \mathbb{R}^{T \times C}$, where T is the number of time points and C is the number of EEG channels. The objective is to learn a meaningful representation \mathbf{h} that can be used to predict the corresponding label $\mathbf{y} \in \mathbb{R}^K$. Here, K denotes the number of target classes with neurological condition, including categories such as Healthy Control (HC), Mild Cognitive Impairment (MCI), Alzheimer’s Disease (AD), Frontotemporal Dementia (FTD), and other brain disorders. In this study, we primarily focus on EEG-based AD detection.

IV. METHOD

A. Overview

Our method incorporates temporal and spatial branches to capture features across two dimensions. The **temporal branch** employs **cross-channel multi-granularity patch embedding**, which embeds patches of varying lengths based on different granularities as tokens for self-attention. The **spatial branch** applies **whole-series multi-granularity channel embedding**: it first scales up the number of channels based on different granularities, then embeds each channel as tokens for self-attention. For both branches, **intra-inter-granularity self-attention** is conducted in two stages. First, intra-granularity self-attention captures local features at different granularities. Then, inter-granularity self-attention, implemented via a router mechanism, learns mutual information across granularities. The two branches operate in parallel. Figure 3 illustrates the overall architecture of our ADformer.

B. Cross-Channel Multi-Granularity Patch Embedding

Considering neuroscience and brain connectivity, there is a naive assumption that inherent correlations exist among different channels in EEG data [60]. *Motivated by this assumption*, we reasonably propose cross-channel patching for token embedding, which captures both temporal and spatial

features in a single step. Figure 1 presents a comparative overview of existing token embedding methods used in other time series tasks and our proposed method. The upper portion illustrates our multi-granularity temporal embedding approach. Additionally, the presence of EEG biomarkers embedded within specific frequency bands [14], [43] further motivates the adoption of multi-granularity embedding. Unlike traditional techniques such as up/downsampling or handcrafted band filtering, multi-granularity learning automatically captures features across different frequency bands.

Given these motivations, we propose a novel token embedding strategy: **cross-channel multi-granularity patch embedding**. Area b) in Figure 3 shows the steps for embeddings. Given a multivariate EEG input sample $x_{\text{in}} \in \mathbb{R}^{T \times C}$ and a set of patch lengths $\{L_1, L_2, \dots, L_n\}$, for the i -th patch length L_i (corresponding to granularity i), we first apply data augmentations to generate augmented views $\tilde{x}_{\text{in}}^{(i)} \in \mathbb{R}^{T \times C}$. Inspired by the contrastive learning framework [61], we argue that such augmentations enhance the learning capacity of the subsequent inter-granularity self-attention stage by promoting knowledge sharing across granularities.

Next, we segment the augmented view $\tilde{x}_{\text{in}}^{(i)}$ into N_i non-overlapping cross-channel patches $x_p^{(i)} \in \mathbb{R}^{N_i \times (L_i \cdot C)}$. Zero padding is applied to ensure that the total number of time steps T is divisible by L_i , yielding $N_i = \lceil T/L_i \rceil$. Each patch is then projected into a latent embedding space via a linear transformation:

$$\mathbf{x}_e^{(i)} = \mathbf{x}_p^{(i)} \mathbf{W}^{(i)}, \quad (1)$$

where $\mathbf{x}_e^{(i)} \in \mathbb{R}^{N_i \times D}$ and $\mathbf{W}^{(i)} \in \mathbb{R}^{(L_i \cdot C) \times D}$.

A fixed positional embedding matrix $\mathbf{W}_{\text{pos}} \in \mathbb{R}^{G \times D}$ is employed for positional encoding [26], where G is a sufficiently large constant. We add the first N_i rows of this matrix, $\mathbf{W}_{\text{pos}}[1 : N_i] \in \mathbb{R}^{N_i \times D}$, along with a learnable granularity embedding $\mathbf{W}_{\text{gr}}^{(i)} \in \mathbb{R}^{1 \times D}$ for the i -th patch length L_i , to form the final patch embedding for granularity i :

$$\mathbf{x}^{(i)} = \mathbf{x}_e^{(i)} + \mathbf{W}_{\text{pos}}[1 : N_i] + \mathbf{W}_{\text{gr}}^{(i)}, \quad (2)$$

where $\mathbf{x}^{(i)} \in \mathbb{R}^{N_i \times D}$. Note that $\mathbf{W}_{\text{gr}}^{(i)}$ is broadcasted to all N_i patch embeddings during addition.

To facilitate interaction across granularities and to reduce computational complexity in subsequent intra-inter-granularity self-attention layers, we also introduce a router token here:

$$\mathbf{u}^{(i)} = \mathbf{W}_{\text{pos}}[N_i + 1] + \mathbf{W}_{\text{gr}}^{(i)}, \quad (3)$$

where $\mathbf{u}^{(i)}, \mathbf{W}_{\text{pos}}[N_i + 1], \mathbf{W}_{\text{gr}}^{(i)} \in \mathbb{R}^{1 \times D}$. Here, $\mathbf{W}_{\text{pos}}[N_i + 1]$ is not used for positional encoding but serves to inform the number of patches at granularity L_i , while $\mathbf{W}_{\text{gr}}^{(i)}$ conveys granularity-specific information. Together, these components distinguish routers associated with different granularities.

In the end, we obtain a set of patch $\{\mathbf{x}^{(1)}, \mathbf{x}^{(2)}, \dots, \mathbf{x}^{(n)}\}$ and router $\{\mathbf{u}^{(1)}, \mathbf{u}^{(2)}, \dots, \mathbf{u}^{(n)}\}$ embeddings corresponding to the patch lengths $\{L_1, L_2, \dots, L_n\}$, collectively denoting multi-granularities. They are fed as input tokens into the subsequent two-stage intra-inter-granularity self-attention module.

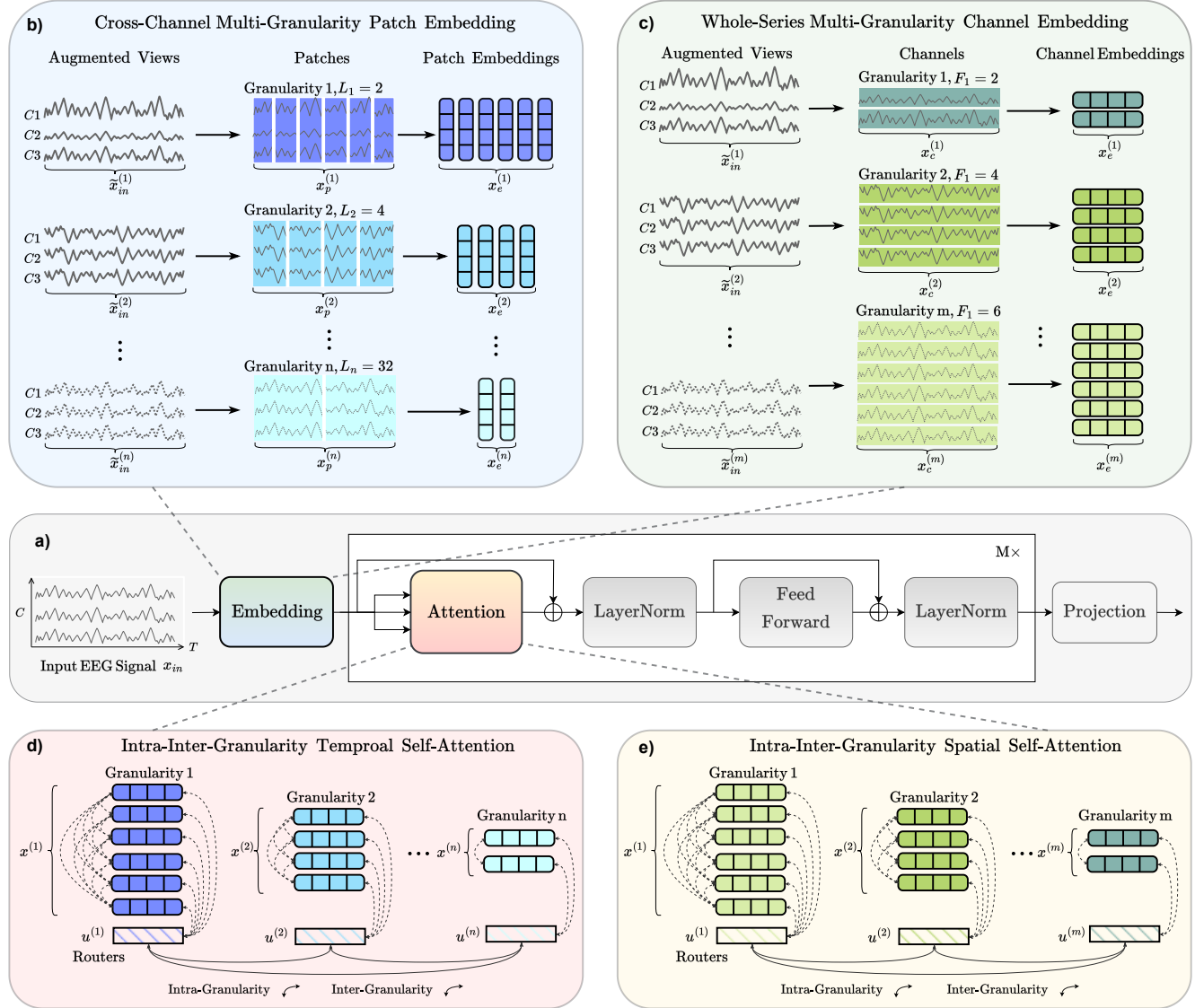


Fig. 3: Overview of ADformer. **a)** Workflow. **b)** For the i -th patch length L_i denoting granularity i and input sample x_{in} , we apply data augmentation to generate the augmented view $\tilde{x}_{in}^{(i)}$ and segment this view into cross-channel non-overlapping patches $x_p^{(i)}$. These patches are mapped into latent space and are combined with granularity and positional embeddings to produce the final patch embedding $x_e^{(i)}$. **c)** For the j -th scaled channel number F_j denoting granularity j and input sample x_{in} , we apply data augmentation to generate the augmented view $\tilde{x}_{in}^{(j)}$. The channel-wise positional embedding is added to the transposed augmented input $(\tilde{x}_{in}^{(j)})^\top$ to get x_{trans} and a linear projection is applied to scale up the channel number. Finally, the entire series of channels is mapped into latent space and combined with the granularity embedding to produce the final channel embedding $x_e^{(j)}$. **d)** and **e)** We compute intra-granularity self-attention, which captures features within individual granularities, and inter-granularity self-attention, allowing for the exchange and learning of information across different granularities. A router mechanism is employed during inter-granularity self-attention to reduce time and space complexity.

C. Whole-Series Multi-Granularity Channel Embedding

Compared to other medical time series data, such as ECG and EMG, EEG signals typically contain more channels due to the electrode system, enabling finer spatial feature representation. To leverage this characteristic, we introduce an additional spatial branch, extending the existing work *Medformer* [32], to better capture spatial features specific to EEG. Unlike the temporal branch, this spatial branch embeds the entire time series of each individual channel as a token. For multi-granularity learning, we scale up the number of channels,

where a larger number of channels corresponds to finer feature utilization and thus represents a finer granularity.

We propose a novel token embedding method: **whole-series multi-granularity channel embedding**, which aims to improve data representation and capture complex channel interactions across different granularity levels. Area c) in Figure 3 shows the steps for embeddings. The lower part of our embedding method in Figure 1 illustrates this embedding method. Given an input multivariate EEG sample $x_{in} \in \mathbb{R}^{T \times C}$, and a list of scaled channel number $\{F_1, F_2, \dots, F_m\}$. For the j -th scaled

channel number F_j denoting granularity j , we first apply data augmentations to obtain augmented input $\tilde{\mathbf{x}}_{\text{in}}^{(j)} \in \mathbb{R}^{T \times C}$. Again, the data augmentation is intended to enhance learning during the inter-granularity self-attention later.

Next, we transpose the input sample and add a fixed channel-wise positional embedding $\mathbf{W}_{\text{pos}}[1 : C]$ to obtain:

$$\mathbf{x}_{\text{trans}} = (\tilde{\mathbf{x}}_{\text{in}}^{(j)})^T + \mathbf{W}_{\text{pos}}[1 : C], \quad (4)$$

where $\mathbf{x}_{\text{trans}}, (\tilde{\mathbf{x}}_{\text{in}}^{(j)})^T, \mathbf{W}_{\text{pos}}[1 : C] \in \mathbb{R}^{C \times T}$. Unlike the temporal branch, here we add positional embedding $\mathbf{W}_{\text{pos}}[1 : C]$ directly to the transposed raw input, as the subsequent channel scaling-up process breaks the original channel order.

We then scale up the channel number using a linear projection $\mathbf{W}_1^{(j)}$ to extract finer spatial features. For scaled channel number F_j denoting granularity j , we obtain $\mathbf{x}_c^j = \mathbf{W}_1^{(j)} \mathbf{x}_{\text{trans}}$, where $\mathbf{x}_c^j \in \mathbb{R}^{F_j \times T}$ and $\mathbf{W}_1^{(j)} \in \mathbb{R}^{T \times C}$. The result \mathbf{x}_c^j is further projected into a latent embedding space using another linear projection: $\mathbf{x}_e^{(j)} = \mathbf{x}_c^{(j)} \mathbf{W}_2^{(j)}$, where $\mathbf{x}_e^{(j)} \in \mathbb{R}^{F_j \times D}$ and $\mathbf{W}_2^{(j)} \in \mathbb{R}^{T \times D}$. Since positional embedding has already been added, we only add a learnable granularity embedding $\mathbf{W}_{\text{gr}}^{(j)} \in \mathbb{R}^{1 \times D}$ to help distinguish the j -th granularity, resulting in the final channel embedding:

$$\mathbf{x}^{(j)} = \mathbf{x}_e^{(j)} + \mathbf{W}_{\text{gr}}^{(j)}, \quad (5)$$

where $\mathbf{x}^{(j)} \in \mathbb{R}^{F_j \times D}$. We also enable a router token here, but only use the granularity embedding $\mathbf{W}_{\text{gr}}^{(j)}$:

$$\mathbf{u}^{(j)} = \mathbf{W}_{\text{gr}}^{(j)}, \quad (6)$$

Finally, we obtain a list of channel $\{\mathbf{x}^{(1)}, \mathbf{x}^{(2)}, \dots, \mathbf{x}^{(m)}\}$ and router $\{\mathbf{u}^{(1)}, \mathbf{u}^{(2)}, \dots, \mathbf{u}^{(m)}\}$ embeddings of different scaled channel numbers $\{F_1, F_2, \dots, F_m\}$, collectively denoting multi-granularities. They are fed as input tokens into the later two-stage intra-inter-granularity self-attention module.

D. Intra-Inter-Granularity Self-Attention

Our goal is to learn multi-granularity features for both the temporal and spatial branch embeddings, while enabling interaction across granularities during self-attention. Taking the temporal branch as an example, a naive approach would be to concatenate all patch embeddings $\{\mathbf{x}^{(1)}, \mathbf{x}^{(2)}, \dots, \mathbf{x}^{(n)}\}$ into a large patch embedding $\mathbf{X} \in \mathbb{R}^{(\sum_{i=1}^n N_i) \times D}$ and perform self-attention on this new embedding, where n denotes the number of different granularities. However, this approach leads to a time complexity of $O((\sum_{i=1}^n N_i)^2)$, which becomes computationally infeasible for large n .

To reduce the computational complexity, we introduce a router mechanism and divide the self-attention process into two distinct stages: a) intra-granularity and b) inter-granularity self-attention. The intra-granularity stage performs self-attention within each individual granularity to capture its unique features. In contrast, the inter-granularity stage performs self-attention across different granularities, enabling the model to learn shared and complementary features across scales. *The intra-inter-granularity self-attention mechanisms for the temporal*

and spatial branches operate independently and do not share parameters, though they follow the same procedural steps. Parts d) and e) in Figure 1 illustrate the intra- and inter-granularity processes for the temporal and spatial branches, respectively.

1) Intra-Granularity Self-Attention: For granularity i , we concatenate the token embedding $\mathbf{x}^{(i)} \in \mathbb{R}^{N_i \times D}$ and router embedding $\mathbf{u}^{(i)} \in \mathbb{R}^{1 \times D}$ to form an intermediate sequence of embeddings $\mathbf{z}^{(i)} \in \mathbb{R}^{(N_i+1) \times D}$:

$$\mathbf{z}^{(i)} = [\mathbf{x}^{(i)} \parallel \mathbf{u}^{(i)}] \quad (7)$$

where $[\cdot \parallel \cdot]$ denotes concatenation. Self-attention is then performed on $\mathbf{z}^{(i)}$ for both the token and router embeddings:

$$\begin{aligned} \mathbf{x}^{(i)} &\leftarrow \text{Attn}^{\text{Intra}}(\mathbf{x}^{(i)}, \mathbf{z}^{(i)}, \mathbf{z}^{(i)}) \\ \mathbf{u}^{(i)} &\leftarrow \text{Attn}^{\text{Intra}}(\mathbf{u}^{(i)}, \mathbf{z}^{(i)}, \mathbf{z}^{(i)}) \end{aligned} \quad (8)$$

where $\text{Attn}^{\text{Intra}}(\mathbf{Q}, \mathbf{K}, \mathbf{V})$ refers to the scaled dot-product attention mechanism described in [26]. The router embedding $\mathbf{u}^{(i)}$ is updated simultaneously with the token embedding $\mathbf{x}^{(i)}$ to ensure consistency. This update allows the router embedding to summarize features at the current training step within the same granularity, while the token embeddings receive global information from the router. The intra-granularity self-attention mechanism helps the model to capture features within the same granularity, facilitating the extraction of local features and correlations among timestamps of the same scale.

2) Inter-Granularity Self-Attention: We concatenate all router embeddings $\{\mathbf{u}^{(1)}, \mathbf{u}^{(2)}, \dots, \mathbf{u}^{(n)}\}$ to form a sequence of routers $\mathbf{U} \in \mathbb{R}^{n \times D}$:

$$\mathbf{U} = [\mathbf{u}^{(1)} \parallel \mathbf{u}^{(2)} \parallel \dots \parallel \mathbf{u}^{(n)}] \quad (9)$$

where n is the number of different granularities. For each granularity i with patch length L_i , we apply self-attention to the router embedding $\mathbf{u}^{(i)} \in \mathbb{R}^{1 \times D}$ with all the routers \mathbf{U} :

$$\mathbf{u}^{(i)} \leftarrow \text{Attn}^{\text{Inter}}(\mathbf{u}^{(i)}, \mathbf{U}, \mathbf{U}) \quad (10)$$

This process enables each router, which already incorporates local features via intra-granularity self-attention, to exchange information with other routers of different granularities. Thus, inter-granularity self-attention effectively captures cross-granularity dependencies and mutual information across various levels. Moreover, the router mechanism significantly reduces the time complexity compared to the naive approach. Taking the temporal branch as an example, the complexity is reduced from $O((\sum_{i=1}^n N_i)^2)$ to $O(\sum_{i=1}^n N_i^2 + n^2)$. Given that $N_i \leq T$, the worst-case time complexity for the intra-inter-granularity temporal self-attention becomes $O(nT^2 + n^2)$, offering a more efficient solution for multi-granularity modeling.

E. Classifier

For a given sample \mathbf{x}_{in} , after M layers of encoding, we obtain a list of updated routers for temporal branch $\mathbf{u}^{(1)}, \mathbf{u}^{(2)}, \dots, \mathbf{u}^{(n)}$ and spatial branch $\mathbf{u}^{(1)}, \mathbf{u}^{(2)}, \dots, \mathbf{u}^{(m)}$, where n and m denote the number of granularities for spatial

TABLE I: Processed Dataset Statistics. All datasets are downsampling to 128Hz, segmented into 1s, half overlapping samples. Abbreviations: **RS** - Resting State; **PS** - Photic Stimulation; **HV** - Hyperventilation. **HC** - Healthy Controls; **AD**: Alzheimer's Disease; **AD**: Alzheimer's Disease; **FTD**: Frontotemporal Dementia; **MCI**: Mild Cognitive Impairment; **SCZ**: Schizophrenia; **DEM**: Depression; **DEM**: Dementia.

Datasets	Task	#Subjects	Sampling Rate	#Channels	#1-s Samples	Classes
ADFTD	RS & PS	88	500->128 Hz	19	191,712	HC & AD & FTD
CNBPM	RS	189	256->128 Hz	19	140,165	HC & AD & MCI
P-ADIC	RS	249	500->128 Hz	19	542,490	HC & AD & MCI & SCZ & DEP
CAUEEG	RS & PS & HV	1187	200->128 Hz	19	1,720,783	HC & DEM & MCI

and temporal branch, respectively. These **router embeddings** are concatenated to form a final representation $h \in \mathbb{R}^{(n+m) \times D}$, which is then passed through a linear classifier to predict the label $\hat{y} \in \mathbb{R}^K$. The model is trained using the cross-entropy loss computed with the ground-truth $y \in \mathbb{R}^K$.

V. EXPERIMENTAL SETUPS

A. Datasets

To demonstrate the end-to-end learning capability of our method for EEG-based Alzheimer's Disease (AD) detection, we utilize four widely used and large-scale datasets that include subjects diagnosed with AD, other brain disorders, and healthy controls. EEG recording tasks in these datasets include resting-state, photic stimulation, and hyperventilation. The datasets used are: **ADFTD**¹² [62], **CNBPM** [63], **P-ADIC**³ [64], and **CAUEEG**⁴ [53], comprising a total of 1,713 subjects. All the subjects are informed consent during data collection according to the readme file of these datasets. We perform artifact removal using Independent Component Analysis (ICA) combined with the ICLabel algorithm [65], which automatically identifies and eliminates components associated with common artifacts such as eye blinks, muscle activity, and heartbeats. A band-pass filter between 0.5 Hz and 45 Hz is applied, and all signals are resampled to 128 Hz. The EEG data from each subject is segmented into 1-second samples with 50% overlap. Z-score normalization is applied to each sample. This results in a total of 2,595,150 processed 1-s samples. Detailed dataset statistics are presented in Table I.

B. Baselines

We compare our method against 8 baselines, including 1 traditional feature-based approach and 7 deep learning models. The feature-based method combines commonly used **Statistical** [10], [11], **Spectral** [12], [13], **Power** [14], [15], and **Complexity** [16], [17] features (in total 32) for EEG-based AD detection, followed by classification using a linear classifier. The deep learning baselines are either state-of-the-art models or have demonstrated strong performance in EEG and medical time series classification tasks. The six deep learning

models include: **EEGNet** [66], **TST** [67], **EEGInception** [68], **EEGConformer** [47], **BIOT** [48], **Medformer** [32], and **MedGNN** [69].

C. Training Settings

Model training is conducted for up to 200 epochs, with early stopping based on validation performance using a patience of 15 epochs, as determined by the best sample-level F1 score. We use a batch size of 512. The optimizer is AdamW with a learning rate of 1e-4. A CosineAnnealingLR scheduler is used to dynamically adjust the learning rate during training. Model performance is evaluated using four metrics: sample-level accuracy, sample-level F1 score, subject-level accuracy, and subject-level F1 score (computed via majority voting, as described in Section III-A). We adopt a Monte Carlo cross-validation strategy [70] with a subject-independent train/validation/test split ratio of 6:2:2 for each dataset. Each experiment is repeated using five different random seeds (41–45), and the mean and standard deviation of the evaluation metrics are reported. All experiments are conducted on a cluster with four NVIDIA A5000 GPUs using Python 3.8 and PyTorch 2.0.0+cu118. Further implementation details are provided in Appendix S.III.

VI. EXPERIMENTAL RESULTS

A. Multi-Class Classification

We begin by performing a multi-class classification task to evaluate our model's ability to detect Alzheimer's Disease (AD) as well as other brain disorders, such as Frontotemporal Dementia (FTD), Mild Cognitive Impairment (MCI), and Schizophrenia (SCZ). The disorder classes associated with each dataset are summarized in Table I. It is worth noting that for the CAUEEG dataset, AD subjects are included within the broader Dementia (DEM) category, which also encompasses other dementia types such as vascular dementia. We retain the original class labels provided by the dataset. In real-world clinical scenarios, brain disorder detection is far more complex than a standard multi-class classification task. One challenge is the potential **comorbid neurological conditions** in a single patient, making the task inherently multi-label in nature. In such cases, each disease class may require a distinct projection head for prediction. Another complication arises from the **overlapping distribution of disorder categories**. For example, some MCI patients eventually progress to AD (referred to as progressive MCI or PMCI), while others remain stable (SMCI) or revert to a healthy condition (HC) [71], [72]. Importantly, PMCI subjects may already exhibit AD-related features at the

¹<https://openneuro.org/datasets/ds004504/versions/1.0.8>

²<https://openneuro.org/datasets/ds006036/versions/1.0.5>

³<https://datadryad.org/dataset/doi:10.5061/dryad.8gtht76pw>

⁴<https://github.com/ipis-mjkim/caueeg-dataset>

TABLE II: Multi-Class Classification Results. All the classes in the datasets are utilized for various brain disorder detection.

Datasets	ADFTD (191,712 Samples) (88 Subjects, 3 Classes)		CNBPM (140,165 Samples) (189 Subjects, 3 Classes)		P-ADIC (542,490 Samples) (249 Subjects, 5 Classes)		CAUEEG (1,720,783 Samples) (1187 Subjects, 3 Classes)	
	Metrics	Accuracy	F1 Score	Accuracy	F1 Score	Accuracy	F1 Score	Accuracy
Sample-Level Classification								
ManualFeature	47.50±2.75	45.02±2.06	53.53±5.67	47.83±5.53	33.25±3.34	24.25±1.82	43.84±2.03	42.60±2.25
EEGNet	49.17±2.31	42.36±2.72	55.27±7.94	47.03±4.80	38.78±1.78	19.20±2.11	45.72±0.63	45.26±0.69
TST	57.20±3.16	54.33±4.51	64.38±5.28	60.45±5.44	32.25±3.68	25.90±3.01	49.08±1.35	48.90±1.56
EEGInception	63.35±1.85	61.61±2.03	63.74±3.58	59.56±3.67	32.01±4.54	25.63±4.05	50.60±1.35	49.85±1.88
EEGConformer	66.21±3.59	63.58±4.35	65.99±4.79	61.97±4.90	33.05±3.85	26.39±2.94	51.41±1.31	51.21±1.55
BIOT	60.96±2.69	58.28±2.52	60.90±6.07	53.77±5.29	33.54±2.55	27.47±2.43	48.65±1.07	48.22±1.62
MedGNN	62.17±2.81	59.98±3.37	67.38±3.70	63.09±3.31	34.44±2.63	27.24±3.15	49.82±1.31	49.63±1.46
Medformer	60.62±4.13	57.54±5.34	66.36±4.22	62.30±4.21	35.07±3.93	27.37±2.35	49.40±0.90	48.80±1.14
ADformer (Ours)	61.92±3.14	59.16±3.89	67.92±3.78	63.51±3.52	35.70±2.71	27.81±1.49	50.49±0.95	50.06±1.23
Subject-Level Detection								
ManualFeature	62.11±3.94	53.35±6.69	55.90±6.96	51.75±7.74	39.23±2.61	21.68±21.68	50.04±4.80	45.62±6.27
EEGNet	60.00±5.37	49.42±7.42	56.41±1.62	52.70±3.97	41.54±3.12	18.81±2.84	50.79±0.86	48.66±0.85
TST	71.58±5.37	68.16±7.32	58.46±9.37	58.39±9.10	40.00±5.22	31.28±4.10	58.41±1.99	57.08±2.64
EEGInception	73.68±3.33	71.14±4.93	60.51±6.80	60.09±6.57	33.46±5.10	24.83±6.52	59.16±1.69	56.49±3.51
EEGConformer	76.84±7.14	72.77±9.08	63.59±2.99	63.58±3.03	36.92±6.37	26.76±3.95	59.75±2.24	58.54±2.17
BIOT	74.74±6.14	72.43±6.77	60.00±3.48	57.17±5.92	39.23±3.96	28.26±3.71	57.15±2.50	55.28±3.66
MedGNN	69.47±6.14	66.06±6.69	64.62±2.99	64.31±3.21	38.46±4.03	26.99±7.41	57.32±1.61	55.99±1.64
Medformer	73.68±5.77	69.72±8.03	62.05±6.96	62.00±6.94	40.38±3.44	29.16±0.80	58.58±1.09	56.45±1.50
ADformer (Ours)	77.89±6.14	74.55±7.51	65.64±4.76	65.88±4.77	44.23±2.72	33.34±1.48	60.67±1.27	59.12±1.73

time of data collection, yet without longitudinal follow-up studies, their future diagnosis remains unknown. In this paper, we simplify the task to a multi-class classification for model evaluation. However, we emphasize that this simplification does not reflect the complexity of real-world scenarios and should be used with caution in practical deployments.

The experimental results are presented in Table II. Our method achieves the best performance in 12 out of 16 reported metrics across the four datasets. In particular, for subject-level metrics—including accuracy and F1 score—our method consistently achieves the top results on all datasets, demonstrating its potential utility in real-world detection settings. The results from CNBPM and CAUEEG support our earlier hypothesis that distinguishing MCI from AD/Dementia can be challenging, likely due to unobserved overlap at the time of data acquisition. The relatively poor performance on P-ADIC suggests that distinguishing between heterogeneous brain disorders such as Schizophrenia (SCZ) and Depression (DEP), when mixed with dementia-related conditions like AD, HC, and MCI, remains difficult. In clinical practice, it may be beneficial to apply preliminary diagnostic filtering by clinicians to exclude non-dementia-related subjects when the target is AD detection. Interestingly, we observe that the best sample-level performance does not always mean the best subject-level results after majority voting. For example, EEGConformer achieves the highest sample-level F1 score on the ADFTD dataset, outperforming our method by 4.42%; however, our method surpasses EEGConformer at the subject level by 1.78% in F1 score. This discrepancy highlights a potential issue: post-processing methods like majority voting are not involved in model training, and merely sample-level training may reveal overfitting to specific subjects during learning. This suggests the need for future work on subject-level regularization strategies

to bridge further the gap between training objectives and evaluation metrics in clinical applications.

B. AD vs HC Classification

We then perform a binary classification task to evaluate the model’s ability to distinguish between Alzheimer’s Disease (AD) and Healthy Control (HC) subjects. AD is the most prevalent neurodegenerative disorder among the elderly and is the primary cause of dementia. Differentiating AD from HC subjects enables us to identify features explicitly associated with AD, as compared to normal aging, which is beneficial for further research on the discovery of early-stage AD patterns in EEG-based detection. As noted previously, in the CAUEEG dataset, AD subjects are grouped under the broader Dementia category, which includes other forms of dementia such as vascular dementia. In contrast, the other three datasets used in this study provide a distinct AD class, allowing for more precise evaluation of AD-specific detection performance.

The results are reported in Table III. Our method achieves the best performance in 12 out of 16 metrics across the four datasets. In particular, the subject-level F1 scores reach approximately 90% for ADFTD and CNBPM, and exceed 80% for CAUEEG, indicating that EEG-based methods can effectively capture discriminative patterns between AD and HC subjects. The relatively lower performance on P-ADIC may be attributed to data quality issues, such as signal contamination from artifacts or inconsistencies in data collection. Additionally, we again observe that the highest sample-level performance does not necessarily lead to the best subject-level results—an observation consistent with our findings from the multi-class classification experiments. This reinforces the importance of evaluating both levels and calls for further research into subject-level alignment

TABLE III: AD/Dementia vs HC Results. The task is Dementia vs HC in CAUEEG and AD vs HC in the other three datasets.

Datasets	ADFTD (147,101 Samples) (65 Subjects, 2 Classes)		CNBPM (92,619 Samples) (126 Subjects, 2 Classes)		P-ADIC (326,898 Samples) (145 Subjects, 2 Classes)		CAUEEG (1,074,469 Samples) (770 Subjects, 2 Classes)	
	Metrics	Accuracy	F1 Score	Accuracy	F1 Score	Accuracy	F1 Score	Accuracy
Sample-Level Classification								
ManualFeature	64.04±3.21	63.48±3.34	68.78±4.65	63.78±5.58	62.14±1.35	57.06±2.26	70.32±1.28	69.91±1.40
EEGNet	64.71±4.12	64.38±4.16	71.38±7.36	67.83±7.09	67.30±3.86	60.74±4.47	68.97±0.99	68.45±1.15
TST	71.28±1.67	71.01±1.68	85.32±5.34	83.24±6.24	62.89±3.09	60.03±2.23	73.86±1.60	73.24±1.89
EEGInception	81.18±2.24	81.06±2.17	86.08±5.12	84.32±5.10	65.31±2.10	59.44±2.02	75.22±1.51	74.75±1.94
EEGConformer	79.71±2.73	79.49±2.75	86.86±5.87	85.38±6.17	63.78±3.39	59.26±2.58	76.73±1.27	76.09±1.61
BIOT	73.85±2.11	73.40±2.61	77.64±5.46	73.65±5.20	65.53±3.47	59.90±3.01	74.50±1.62	73.99±1.85
MedGNN	79.11±2.50	79.06±2.50	86.78±4.52	84.57±5.73	64.09±2.62	59.10±1.66	75.70±1.60	74.97±1.97
Medformer	75.30±3.30	75.03±3.10	85.42±6.18	83.63±6.98	64.94±2.49	61.31±1.61	74.34±1.43	73.59±1.86
ADformer (Ours)	75.84±2.20	75.73±2.19	88.05±3.76	86.21±4.56	65.34±3.57	61.65±2.25	76.21±1.62	75.62±1.96
Subject-Level Detection								
ManualFeature	81.43±5.71	80.33±6.23	73.08±11.67	69.97±15.96	68.00±3.40	59.18±6.92	80.39±1.76	79.39±1.84
EEGNet	78.57±7.82	78.04±7.92	79.23±6.71	78.34±7.84	72.00±4.99	61.83±8.38	77.03±1.61	75.87±2.14
TST	85.71±7.82	85.52±8.03	84.62±10.03	84.39±10.09	68.67±4.00	64.71±5.26	83.48±1.66	82.14±2.30
EEGInception	91.43±2.86	91.34±2.81	86.92±5.76	86.63±6.21	71.33±4.00	64.43±3.70	83.74±1.70	82.72±2.28
EEGConformer	91.43±5.35	91.35±5.41	87.69±10.15	87.64±10.21	68.00±4.52	60.00±7.40	85.29±1.93	84.22±2.37
BIOT	90.00±5.71	89.83±5.68	83.08±3.92	82.80±4.18	73.33±5.58	65.72±7.63	83.23±1.96	82.12±2.31
MedGNN	90.00±3.50	89.92±3.56	86.92±6.25	86.89±6.24	67.33±4.90	61.28±3.41	84.00±2.43	82.69±3.04
Medformer	90.00±3.50	89.86±3.51	85.38±8.21	85.08±8.40	71.33±1.63	66.95±2.91	83.10±1.70	81.60±2.31
ADformer (Ours)	92.86±0.00	92.82±0.00	90.00±6.25	89.83±6.48	72.00±5.81	67.99±6.57	85.55±2.52	84.42±3.06

and training strategies to improve consistency between sample-level learning and subject-level outcomes.

C. Ablation Study

To evaluate the effectiveness of each component in our proposed method, we conduct an ablation study by systematically removing individual modules and assessing the resulting performance changes. Specifically, we evaluate the impact of removing the **inter-granularity self-attention**, the **temporal branch**, and the **spatial branch**. The performance of the complete model (with all modules included) is also reported for comparison. The parameters for **all modules utilized** are the same as parameter choices in Table III.

The results are summarized in Table IV, and Figure 4 provides a visual comparison of the different model variants. For 3 out of the 4 datasets, the full model achieves the highest subject-level F1 score, demonstrating the complementary contributions of the proposed components. Across all datasets, both the temporal and spatial branches significantly enhance performance; removing either branch leads to a clear performance drop, highlighting the importance of modeling both temporal dynamics and spatial channel relationships in EEG data. Notably, the inter-granularity self-attention module does not consistently improve performance in all cases. For instance, in the P-ADIC dataset, its removal yields comparable or even slightly better results. This may be due to the limited number of granularity levels in this dataset, making it difficult for the model to learn meaningful inter-granularity relationships. Overall, the ablation study confirms that each module in our model design contributes positively to performance in most scenarios, validating the architecture choices of ADformer.

D. Sample Length & Overlapping Study

Sample length and overlapping rate are two critical parameters in EEG data segmentation. Appropriate choices of these parameters can help preserve essential temporal and frequency features while also increasing the amount of training data available for deep learning models. Since our ultimate goal is to detect whether a subject has AD based on aggregated sample-level predictions, it is important to explore how different sample lengths and overlapping rates affect subject-level performance in EEG-based AD detection. To this end, we evaluate the binary classification task of AD/Dementia vs. HC on two publicly available datasets—ADFTD and CAUEEG, which have shown relatively strong performance in this task. We evaluate 3 different sample lengths: 128(1s), 256(2s), 512(4s), and 1024(8s) timestamps. We then fix the sample length to 128 and change the overlapping rate across 0%, 20%, 50%, and 80%. For simplicity, we fix the patch length L_i to 4 and the scaled channel number F_j to 76, adopting a single-granularity setup across all experiments.

The results are summarized in Table V and Table VI. Figure 5 and Figure 6 further illustrate the performance comparison and trend under varying sample lengths and overlapping rates. For sample length, the best performance, in terms of both sample-level and subject-level F1 scores, is observed at 128 and 256 timestamps on the two datasets. **This suggests that arbitrarily increasing sample length does not necessarily improve overall performance**, likely due to a reduction in the number of training samples, which can negatively impact learning. For the overlapping rate, we observe that a 50% overlap consistently yields the best results for both sample-level and subject-level metrics across datasets, with one exception at 80% overlap. In general, using overlapping segmentation outperforms the non-overlapping (0%) result. Although the

TABLE IV: **Ablation Study.** Effectiveness of each module of our method on the AD/Dementia vs HC task.

Datasets	ADFTD (147,101 Samples) (65 Subjects, 2 Classes)		CNBPM (92,619 Samples) (126 Subjects, 2 Classes)		P-ADIC (326,898 Samples) (145 Subjects, 2 Classes)		CAUEEG (1,074,469 Samples) (770 Subjects, 2 Classes)	
Metrics Methods	Accuracy	F1 Score	Accuracy	F1 Score	Accuracy	F1 Score	Accuracy	F1 Score
Sample-Level Classification								
No Inter-Attention	77.32±1.89	77.21±1.83	86.36±4.67	84.57±5.40	65.80±3.87	61.80±1.90	76.13±1.60	75.56±1.88
No Temporal Branch	74.06±3.70	73.63±3.84	86.43±3.46	84.19±3.97	65.13±2.00	57.55±5.36	75.56±1.28	74.84±1.61
No Spatial Branch	75.02±2.42	74.88±2.33	87.50±4.62	85.79±5.31	64.82±4.61	61.75±3.10	75.39±1.40	74.66±1.75
All Module Utilized	75.84±2.20	75.73±2.19	88.05±3.76	86.21±4.56	65.34±3.57	61.65±2.25	76.21±1.62	75.62±1.96

Subject-Level Detection								
No Inter-Attention	91.43±2.86	91.34±2.96	86.15±4.62	85.98±4.78	73.33±4.22	68.25±5.17	85.16±1.87	84.05±2.27
No Temporal Branch	85.71±4.52	85.31±4.56	86.15±5.22	86.11±5.22	67.33±5.73	54.98±12.97	83.87±2.86	82.57±3.33
No Spatial Branch	90.00±3.50	89.86±3.63	89.23±6.15	88.96±6.67	71.33±7.48	67.13±7.23	83.87±2.74	82.50±3.19
All Module Utilized	92.86±0.00	92.82±0.00	90.00±6.25	89.83±6.48	72.00±5.81	67.99±6.57	85.55±2.52	84.42±3.06

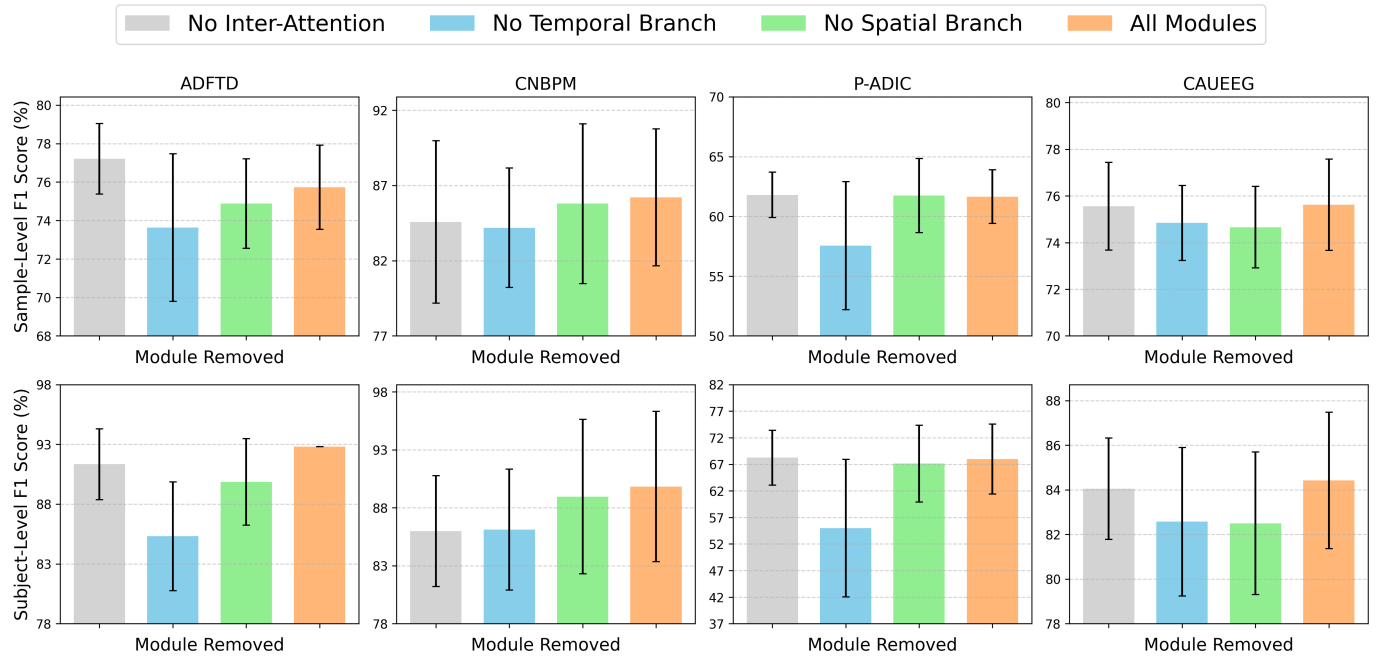


Fig. 4: The ablation study of different modules removed.

TABLE V: **Sample Length Study.** We evaluate how different sample lengths T impact the performance of ADFTD and CAUEEG on the AD/Dementia vs HC task.

Datasets	ADFTD (147,101 Samples) (65 Subjects, 2 Classes)		CAUEEG (1,074,469 Samples) (770 Subjects, 2 Classes)	
Metrics Lengths	Accuracy	F1 Score	Accuracy	F1 Score
Sample-Level Classification				
128 (1s)	74.49±3.18	74.28±3.39	75.70±1.43	74.98±1.74
256 (2s)	74.59±3.40	74.40±3.47	76.04±1.56	75.34±2.00
512 (4s)	74.63±3.81	74.28±4.02	75.64±1.80	74.77±2.12
1024 (8s)	70.47±6.08	69.92±5.98	75.02±1.91	74.20±2.20
Subject-Level Detection				
128 (1s)	88.57±3.50	88.44±3.58	84.52±2.34	83.31±2.65
256 (1s)	88.57±3.50	88.44±3.58	83.87±1.87	82.51±2.48
512 (1s)	87.14±8.33	86.55±9.24	82.19±1.94	80.68±2.19
1024 (8s)	87.14±5.35	86.74±5.55	80.90±1.33	79.24±1.62

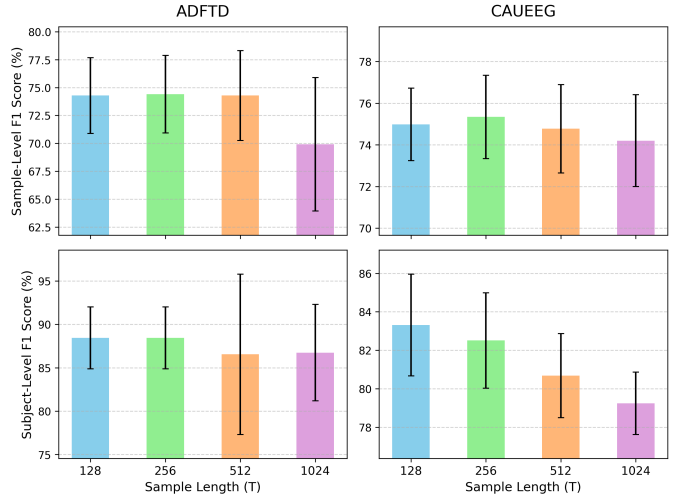


Fig. 5: The results comparison of different sample lengths.

TABLE VI: Overlapping Rate Study. We evaluate how different sample overlapping ratios impact the performance of ADFTD and CAUEEG on the AD/Dementia vs HC task.

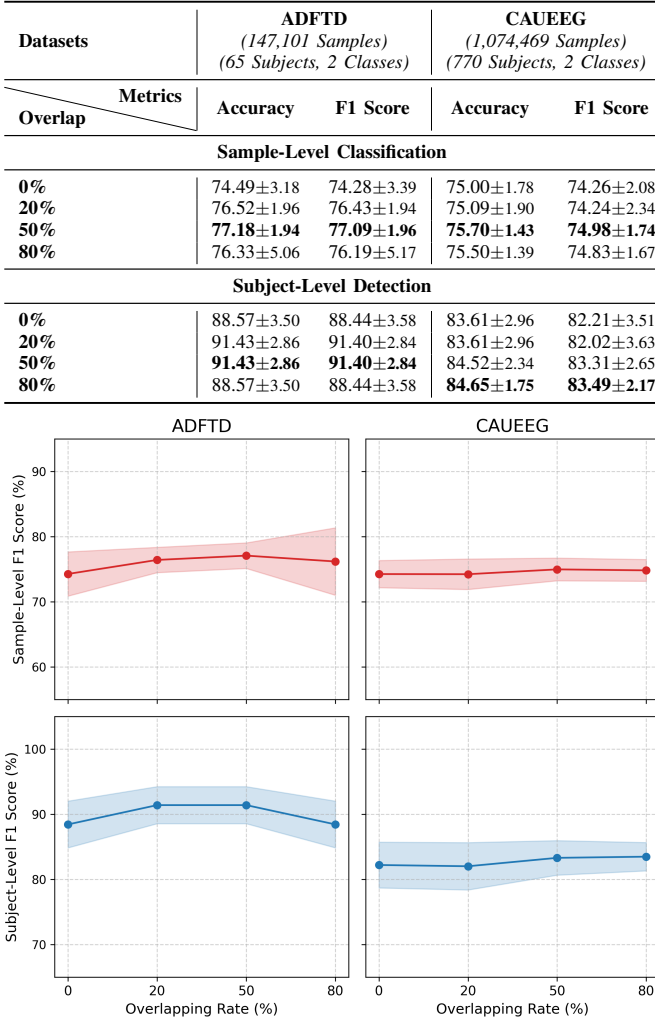


Fig. 6: The results comparison of different overlapping rates.

effectiveness of overlapping segmentation in self-supervised learning remains uncertain, our findings clearly demonstrate that **applying sample overlap—regardless of the specific rate—improves performance in supervised learning for EEG-based AD detection.**

VII. CONCLUSION AND FUTURE WORKS

This paper introduces **ADformer**, a novel end-to-end multi-granularity spatial-temporal transformer designed for EEG-based Alzheimer’s Disease (AD) detection. We propose two innovative multi-granularity data embedding strategies that effectively capture both temporal and spatial features. In addition, we design a two-stage intra-inter granularity self-attention mechanism to extract local patterns within each granularity and global dependencies across granularities. We conduct comprehensive evaluations on four large-scale EEG datasets, comprising a total of 1,713 subjects and 2,595,150 one-second samples. Experiments include both multi-class classification among various brain disorders and binary classification between AD and healthy control (HC) subjects. To

simulate real-world clinical scenarios, we employ a subject-independent cross-validation protocol and apply majority voting to aggregate sample-level predictions into subject-level detections. Our findings show that distinguishing dementia-related disorders from other brain disorders such as schizophrenia and depression remains challenging, indicating the potential need for pre-screening by clinicians to filter out unrelated diagnoses. In contrast, binary classification between AD and HC yields strong results, with subject-level F1 scores reaching around 90% on several datasets. Additionally, we explore how segmentation parameters—specifically sample length and overlapping rate—affect subject-level performance. Our results suggest that longer sample lengths do not necessarily lead to better performance and may degrade it. On the other hand, applying sample overlapping during segmentation, regardless of the specific overlap rate, consistently improves subject-level detection performance.

We identify two promising directions for future research: 1) **Adaptive Granularity Selection.** In this work, the granularity levels for patch length and scaled channel number are manually tuned, which can be time-consuming and suboptimal across datasets. Incorporating a mixture-of-experts mechanism may enable the model to dynamically select the most appropriate granularity levels based on dataset characteristics, thereby improving both flexibility and performance. 2) **Subject-Level Regularization.** Our results reveal that the best sample-level performance does not always imply the best subject-level performance after majority voting. This discrepancy suggests the need for subject-aware training strategies. Future work could explore subject-level regularization methods that backpropagate subject-level prediction errors to guide model optimization, potentially improving overall subject-level robustness.

REFERENCES

- [1] Zeinab Breijeh and Rafik Karaman. Comprehensive review on alzheimer’s disease: Causes and treatment. *Molecules*, 25(24):5789, 2020.
- [2] Colin L Masters, Randall Bateman, Kaj Blennow, Christopher C Rowe, Reisa A Sperling, and Jeffrey L Cummings. Alzheimer’s disease. *Nature reviews disease primers*, 1(1):1–18, 2015.
- [3] M Paul Murphy and Harry LeVine III. Alzheimer’s disease and the amyloid- β peptide. *Journal of Alzheimer’s disease*, 19(1):311–323, 2010.
- [4] Lucy Nelson and Naji Tabet. Slowing the progression of alzheimer’s disease; what works? *Ageing research reviews*, 23:193–209, 2015.
- [5] LW Chu. Alzheimer’s disease: early diagnosis and treatment. *Hong Kong Medical Journal*, 18(3):228, 2012.
- [6] Joon Ho Choi, Hyun-Ah Kim, Wook Kim, Ilhan Lim, Inki Lee, Byung Hyun Byun, Woo Chul Noh, Min-Ki Seong, Seung-Sook Lee, Byung Il Kim, et al. Early prediction of neoadjuvant chemotherapy response for advanced breast cancer using pet/mri image deep learning. *Scientific reports*, 10(1):21149, 2020.
- [7] Claes Nøhr Ladefoged, Lisbeth Marner, Amalie Hindsholm, Ian Law, Liselotte Høgaard, and Flemming Littrup Andersen. Deep learning based attenuation correction of pet/mri in pediatric brain tumor patients: evaluation in a clinical setting. *Frontiers in neuroscience*, 12:1005, 2019.
- [8] Katerina D Tzimourta, Vasileios Christou, Alexandros T Tzallas, Nikolaos Giannakeas, Loukas G Astrakas, Pantelis Angelidis, Dimitrios Tsalikakis, and Markos G Tsipouras. Machine learning algorithms and statistical approaches for alzheimer’s disease analysis based on resting-state eeg recordings: A systematic review. *International journal of neural systems*, 31(05):2130002, 2021.

[9] Cosimo Ieracitano, Nadia Mammone, Alessia Bramanti, Amir Hussain, and Francesco C Morabito. A convolutional neural network approach for classification of dementia stages based on 2d-spectral representation of eeg recordings. *Neurocomputing*, 323:96–107, 2019.

[10] Katerina D Tzimourta, Nikolaos Giannakeas, Alexandros T Tzallas, Loukas G Astrakas, Theodora Afrantou, Panagiotis Ioannidis, Nikolaos Grigoriadis, Pantelis Angelidis, Dimitrios G Tsalikakis, and Markos G Tsipouras. Eeg window length evaluation for the detection of alzheimer’s disease over different brain regions. *Brain sciences*, 9(4):81, 2019.

[11] Katerina D Tzimourta, Theodora Afrantou, Panagiotis Ioannidis, Maria Karatzikou, Alexandros T Tzallas, Nikolaos Giannakeas, Loukas G Astrakas, Pantelis Angelidis, Evripidis Glavas, Nikolaos Grigoriadis, et al. Analysis of electroencephalographic signals complexity regarding alzheimer’s disease. *Computers & Electrical Engineering*, 76:198–212, 2019.

[12] Jing Wang, Yuxing Fang, Xiao Wang, Huichao Yang, Xin Yu, and Huali Wang. Enhanced gamma activity and cross-frequency interaction of resting-state electroencephalographic oscillations in patients with alzheimer’s disease. *Frontiers in aging neuroscience*, 9:243, 2017.

[13] Raymundo Cassani, Tiago H Falk, Francisco J Fraga, Paulo AM Kanda, and Renato Anghinah. The effects of automated artifact removal algorithms on electroencephalography-based alzheimer’s disease diagnosis. *Frontiers in aging neuroscience*, 6:55, 2014.

[14] Golshan Fahimi, Seyed Mahmoud Tabatabaei, Elnaz Fahimi, and Hamid Rajabi. Index of theta/alpha ratio of the quantitative electroencephalogram in alzheimer’s disease: a case-control study. *Acta Medica Iranica*, pages 502–506, 2017.

[15] Magali T Schmidt, Paulo AM Kanda, Luis FH Basile, Helder Frederico da Silva Lopes, Regina Baratho, Jose LC Demario, Mario S Jorge, Antonio E Nardi, Sergio Machado, Jéssica N Ianof, et al. Index of alpha/theta ratio of the electroencephalogram: a new marker for alzheimer’s disease. *Frontiers in aging neuroscience*, 5:60, 2013.

[16] Heinrich Garn, Markus Waser, Manfred Deistler, Thomas Benke, Peter Dal-Bianco, Gerhard Ransmayr, Helena Schmidt, Guenter Sanin, Peter Santer, Georg Caravias, et al. Quantitative eeg markers relate to alzheimer’s disease severity in the prospective dementia registry austria (prodem). *Clinical Neurophysiology*, 126(3):505–513, 2015.

[17] Hamed Azami, Steven E Arnold, Saeid Sanei, Zhuoqing Chang, Guillermo Sapiro, Javier Escudero, and Anoopam S Gupta. Multiscale fluctuation-based dispersion entropy and its applications to neurological diseases. *IEEE Access*, 7:68718–68733, 2019.

[18] Fangzhou Li, Shoya Matsumori, Naohiro Egawa, Shusuke Yoshimoto, Kotaro Yamashiro, Haruo Mizutani, Noriko Uchida, Atsuko Kokuryu, Akira Kuzuya, Ryosuke Kojima, et al. Predictive diagnostic approach to dementia and dementia subtypes using wireless and mobile electroencephalography: A pilot study. *Bioelectricity*, 4(1):3–11, 2022.

[19] Ozlem Karabiber Cura, Gulce C Yilmaz, H Sabiha Ture, and Aydin Akan. Deep time-frequency feature extraction for alzheimer’s dementia eeg classification. In 2022 Medical Technologies Congress (TIPTEKNO), pages 1–4. IEEE, 2022.

[20] Xiaocai Shan, Jun Cao, Shoudong Huo, Liangyu Chen, Ptolemaios Georgios Sarrigiannis, and Yifan Zhao. Spatial-temporal graph convolutional network for alzheimer classification based on brain functional connectivity imaging of electroencephalogram. *Human Brain Mapping*, 43(17):5194–5209, 2022.

[21] Dominik Klepl, Fei He, Min Wu, Daniel J Blackburn, and Ptolemaios Sarrigiannis. Adaptive gated graph convolutional network for explainable diagnosis of alzheimer’s disease using eeg data. *IEEE Transactions on Neural Systems and Rehabilitation Engineering*, 2023.

[22] Andreas Miltiadous, Emmanouil Giannidis, Katerina D Tzimourta, Nikolaos Giannakeas, and Alexandros T Tzallas. Dice-net: a novel convolution-transformer architecture for alzheimer detection in eeg signals. *IEEE Access*, 2023.

[23] Mario Alejandro Bravo-Ortiz, Ernesto Guevara-Navarro, Sergio Alejandro Holguín-García, Mariana Rivera-García, Oscar Cardona-Morales, Gonzalo A Ruz, and Reinel Tabares-Soto. Spectrocvt-net: A convolutional vision transformer architecture and channel attention for classifying alzheimer’s disease using spectrograms. *Computers in Biology and Medicine*, 181:109022, 2024.

[24] Cameron J Huggins, Javier Escudero, Mario A Parra, Brian Scally, Renato Anghinah, Amanda Vitória Lacerda De Araújo, Luis F Basile, and Daniel Abasolo. Deep learning of resting-state electroencephalogram signals for three-class classification of alzheimer’s disease, mild cognitive impairment and healthy ageing. *Journal of Neural Engineering*, 18(4):046087, 2021.

[25] Marcos Aviles, Luz María Sánchez-Reyes, José Manuel Álvarez-Alvarado, and Juvenal Rodríguez-Reséndiz. Machine and deep learning trends in eeg-based detection and diagnosis of alzheimer’s disease: A systematic review. *Eng*, 5(3):1464–1484, 2024.

[26] Ashish Vaswani, Noam Shazeer, Niki Parmar, Jakob Uszkoreit, Llion Jones, Aidan N Gomez, Łukasz Kaiser, and Illia Polosukhin. Attention is all you need. *Advances in neural information processing systems*, 30, 2017.

[27] Haixu Wu, Jiehui Xu, Jianmin Wang, and Mingsheng Long. Autoformer: Decomposition transformers with auto-correlation for long-term series forecasting. *Advances in Neural Information Processing Systems*, 34:22419–22430, 2021.

[28] Haoyi Zhou, Shanghang Zhang, Jieqi Peng, Shuai Zhang, Jianxin Li, Hui Xiong, and Wancai Zhang. Informer: Beyond efficient transformer for long sequence time-series forecasting. In *Proceedings of the AAAI conference on artificial intelligence*, volume 35, pages 11106–11115, 2021.

[29] Yong Liu, Tengge Hu, Haoran Zhang, Haixu Wu, Shiyu Wang, Lintao Ma, and Mingsheng Long. itransformer: Inverted transformers are effective for time series forecasting. *International Conference on Learning Representations*, 2024.

[30] Yuqi Nie, Nam H Nguyen, Phanwadee Sinthong, and Jayant Kalagnanam. A time series is worth 64 words: Long-term forecasting with transformers. *ICLR*, 2023.

[31] Yunhao Zhang and Junchi Yan. Crossformer: Transformer utilizing cross-dimension dependency for multivariate time series forecasting. In *The Eleventh International Conference on Learning Representations*, 2022.

[32] Yihe Wang, Nan Huang, Taida Li, Yujun Yan, and Xiang Zhang. Medformer: A multi-granularity patching transformer for medical time-series classification. *Advances in Neural Information Processing Systems*, 37:36314–36341, 2024.

[33] NN Kulkarni and VK Bairagi. Extracting salient features for eeg-based diagnosis of alzheimer’s disease using support vector machine classifier. *IETE Journal of Research*, 63(1):11–22, 2017.

[34] Paulo Afonso Medeiros Kanda, Lucas R Trambaiolli, Ana C Lorena, Francisco J Fraga, Luis Fernando I Basile, Ricardo Nitrini, and Renato Anghinah. Clinician’s road map to wavelet eeg as an alzheimer’s disease biomarker. *Clinical EEG and neuroscience*, 45(2):104–112, 2014.

[35] Markus Waser, Manfred Deistler, Heinrich Garn, Thomas Benke, Peter Dal-Bianco, Gerhard Ransmayr, Dieter Grossegger, and Reinhold Schmidt. Eeg in the diagnostics of alzheimer’s disease. *Statistical Papers*, 54:1095–1107, 2013.

[36] Lucie Tylova, Jaromír Kukal, and Oldřich Vysata. Predictive models in diagnosis of alzheimer’s disease from eeg. *Acta Polytechnica*, 53(2), 2013.

[37] Aldo Mora-Sánchez, Gérard Dreyfus, and François-Benoît Vialatte. Scale-free behaviour and metastable brain-state switching driven by human cognition, an empirical approach. *Cognitive neurodynamics*, 13:437–452, 2019.

[38] Ruofan Wang, Jiang Wang, Shunan Li, Haitao Yu, Bin Deng, and Xile Wei. Multiple feature extraction and classification of electroencephalograph signal for alzheimers’ with spectrum and bispectrum. *Chaos: An Interdisciplinary Journal of Nonlinear Science*, 25(1), 2015.

[39] Francisco J Fraga, Tiago H Falk, Paulo AM Kanda, and Renato Anghinah. Characterizing alzheimer’s disease severity via resting-awake eeg amplitude modulation analysis. *PloS one*, 8(8):e72240, 2013.

[40] Luke Tait, George Stothart, Elizabeth Coulthard, Jon T Brown, Nina Kazanina, and Marc Goodfellow. Network substrates of cognitive impairment in alzheimer’s disease. *Clinical Neurophysiology*, 130(9):1581–1595, 2019.

[41] Markus Waser, Heinrich Garn, Reinhold Schmidt, Thomas Benke, Peter Dal-Bianco, Gerhard Ransmayr, Helena Schmidt, Stephan Seiler, Günter Sanin, Florian Mayer, et al. Quantifying synchrony patterns in the eeg of alzheimer’s patients with linear and non-linear connectivity markers. *Journal of Neural Transmission*, 123:297–316, 2016.

[42] Lucas R Trambaiolli, Ana C Lorena, Francisco J Fraga, Paulo AM Kanda, Renato Anghinah, and Ricardo Nitrini. Improving alzheimer’s disease diagnosis with machine learning techniques. *Clinical EEG and neuroscience*, 42(3):160–165, 2011.

[43] Xiaokun Liu, Chunlai Zhang, Zheng Ji, Yi Ma, Xiaoming Shang, Qi Zhang, Wencheng Zheng, Xia Li, Jun Gao, Ruofan Wang, et al. Multiple characteristics analysis of alzheimer’s electroencephalogram by power spectral density and lempel-ziv complexity. *Cognitive neurodynamics*, 10:121–133, 2016.

[44] Lucie Tylová, Jaromír Kukal, Václav Hubata-Vacek, and Oldřich Vysata. Unbiased estimation of permutation entropy in eeg analysis for alzheimer’s disease classification. *Biomedical Signal Processing and Control*, 39:424–430, 2018.

[45] Mohamed Ismail, Klaus Hofmann, and Mohamed A Abd El Ghany. Early diagnoses of alzheimer using eeg data and deep neural networks classification. In *2019 IEEE Global Conference on Internet of Things (GCIoT)*, pages 1–5. IEEE, 2019.

[46] Jin Xie, Jie Zhang, Jiayao Sun, Zheng Ma, Liuni Qin, Guanglin Li, Huihui Zhou, and Yang Zhan. A transformer-based approach combining deep learning network and spatial-temporal information for raw eeg classification. *IEEE Transactions on Neural Systems and Rehabilitation Engineering*, 30:2126–2136, 2022.

[47] Yonghao Song, Qingqing Zheng, Bingchuan Liu, and Xiaorong Gao. Eeg conformer: Convolutional transformer for eeg decoding and visualization. *IEEE Transactions on Neural Systems and Rehabilitation Engineering*, 31:710–719, 2022.

[48] Chaoli Yang, M Westover, and Jimeng Sun. Biot: Biosignal transformer for cross-data learning in the wild. *Advances in Neural Information Processing Systems*, 36, 2024.

[49] Wei-Bang Jiang, Li-Ming Zhao, and Bao-Liang Lu. Large brain model for learning generic representations with tremendous eeg data in bci. *The Twelfth International Conference on Learning Representations*, 2024.

[50] Guangyu Wang, Wenchao Liu, Yuhong He, Cong Xu, Lin Ma, and Haifeng Li. Eegpt: Pretrained transformer for universal and reliable representation of eeg signals. *Advances in Neural Information Processing Systems*, 2024.

[51] Yuqi Chen, Kan Ren, Kaitao Song, Yansen Wang, Yifan Wang, Dongsheng Li, and Lili Qiu. Eegformer: Towards transferable and interpretable large-scale eeg foundation model. *arXiv preprint arXiv:2401.10278*, 2024.

[52] Jiquan Wang, Sha Zhao, Zhiling Luo, Yangxuan Zhou, Haiteng Jiang, Shijian Li, Tao Li, and Gang Pan. Cbramod: A criss-cross brain foundation model for eeg decoding. *ICLR*, 2025.

[53] Min-jae Kim, Young Chul Youn, and Joonki Paik. Deep learning-based eeg analysis to classify normal, mild cognitive impairment, and dementia: Algorithms and dataset. *NeuroImage*, 272:120054, 2023.

[54] Sajeev Kunjan, Tyler S Grummett, Kenneth J Pope, David MW Powers, Sean P Fitzgibbon, T Bastiampillai, M Battersby, and Trent W Lewis. The necessity of leave one subject out (losos) cross validation for eeg disease diagnosis. In *Brain Informatics: 14th International Conference, BI 2021, Virtual Event, September 17–19, 2021, Proceedings 14*, pages 558–567. Springer, 2021.

[55] Majid Nour, Umit Senturk, and Kemal Polat. A novel hybrid model in the diagnosis and classification of alzheimer’s disease using eeg signals: Deep ensemble learning (del) approach. *Biomedical Signal Processing and Control*, 89:105751, 2024.

[56] Dileep kumar Ravikanti and S Saravanan. Eegalzheimer’snet: Development of transformer-based attention long short term memory network for detecting alzheimer disease using eeg signal. *Biomedical Signal Processing and Control*, 86:105318, 2023.

[57] Yusuke Watanabe, Yuki Miyazaki, Masahiro Hata, Ryohei Fukuma, Yasunori Aoki, Hiroaki Kazui, Toshihiko Araki, Daiki Taomoto, Yuto Satake, Takashi Suehiro, et al. A deep learning model for the detection of various dementia and mci pathologies based on resting-state electroencephalography data: A retrospective multicentre study. *Neural Networks*, 171:242–250, 2024.

[58] Sheng Chen, Chutian Zhang, Hongjun Yang, Liang Peng, Haiqun Xie, Zeping Lv, and Zeng-Guang Hou. A multi-modal classification method for early diagnosis of mild cognitive impairment and alzheimer’s disease using three paradigms with various task difficulties. *IEEE Transactions on Neural Systems and Rehabilitation Engineering*, 32:1456–1465, 2024.

[59] Yihe Wang, Yu Han, Haishuai Wang, and Xiang Zhang. Contrast everything: A hierarchical contrastive framework for medical time-series. *Advances in Neural Information Processing Systems*, 36, 2023.

[60] Vincent Bazinet, Justine Y Hansen, and Bratislav Misic. Towards a biologically annotated brain connectome. *Nature reviews neuroscience*, 24(12):747–760, 2023.

[61] Ting Chen, Simon Kornblith, Mohammad Norouzi, and Geoffrey Hinton. A simple framework for contrastive learning of visual representations. In *International conference on machine learning*, pages 1597–1607. PMLR, 2020.

[62] Andreas Miltiadous, Katerina D Tzimourta, Theodora Afrantou, Panagiotis Ioannidis, Nikolaos Grigoriadis, Dimitrios G Tsalikakis, Pantelis Angelidis, Markos G Tsipouras, Euripidis Glavas, Nikolaos Giannakeas, et al. A dataset of scalp eeg recordings of alzheimer’s disease, frontotemporal dementia and healthy subjects from routine eeg. *Data*, 8(6):95, 2023.

[63] Juan P Amezquita-Sanchez, Nadia Mammone, Francesco C Morabito, Silvia Marino, and Hojjat Adeli. A novel methodology for automated differential diagnosis of mild cognitive impairment and the alzheimer’s disease using eeg signals. *Journal of neuroscience methods*, 322:88–95, 2019.

[64] Oded Shor, Amir Glik, Amit Yaniv-Rosenfeld, Avi Valevski, Abraham Weizman, Andrei Khrennikov, and Felix Benninger. Eeg p-adic quantum potential accurately identifies depression, schizophrenia and cognitive decline. *Plos one*, 16(8):e0255529, 2021.

[65] Luca Pion-Tonachini, Ken Kreutz-Delgado, and Scott Makeig. Iclabel: An automated electroencephalographic independent component classifier, dataset, and website. *NeuroImage*, 198:181–197, 2019.

[66] Vernon J Lawhern, Amelia J Solon, Nicholas R Waytowich, Stephen M Gordon, Chou P Hung, and Brent J Lance. Eegnet: a compact convolutional neural network for eeg-based brain-computer interfaces. *Journal of neural engineering*, 15(5):056013, 2018.

[67] George Zerveas, Srideepika Jayaraman, Dhaval Patel, Anuradha Bhamidi-paty, and Carsten Eickhoff. A transformer-based framework for multivariate time series representation learning. In *Proceedings of the 27th ACM SIGKDD conference on knowledge discovery & data mining*, pages 2114–2124, 2021.

[68] Ce Zhang, Young-Keun Kim, and Azim Eskandarian. Eeg-inception: an accurate and robust end-to-end neural network for eeg-based motor imagery classification. *Journal of Neural Engineering*, 18(4):046014, 2021.

[69] Wei Fan, Jingru Fei, Dingyu Guo, Kun Yi, Xiaozhuang Song, Haolong Xiang, Hangting Ye, and Min Li. Towards multi-resolution spatiotemporal graph learning for medical time series classification. In *Proceedings of the ACM on Web Conference 2025*, pages 5054–5064, 2025.

[70] Qing-Song Xu and Yi-Zeng Liang. Monte carlo cross validation. *Chemometrics and Intelligent Laboratory Systems*, 56(1):1–11, 2001.

[71] Fabrizio Vecchio, Francesca Miraglia, Francesco Iberite, Giordano Lacidogna, Valeria Guglielmi, Camillo Marra, Patrizio Pasqualetti, Francesco Danilo Tiziano, and Paolo Maria Rossini. Sustainable method for alzheimer dementia prediction in mild cognitive impairment: Electroencephalographic connectivity and graph theory combined with apolipoprotein e. *Annals of neurology*, 84(2):302–314, 2018.

[72] Yingfeng Ge, Jianan Yin, Caike Chen, Shuo Yang, Yuduan Han, Chonglong Ding, Jiaming Zheng, Yifan Zheng, and Jinxin Zhang. An eeg-based framework for automated discrimination of conversion to alzheimer’s disease in patients with amnestic mild cognitive impairment: an 18-month longitudinal study. *Frontiers in Aging Neuroscience*, 16:1470836, 2025.

[73] Cosimo Ieracitano, Nadia Mammone, Alessia Bramanti, Silvia Marino, Amir Hussain, and Francesco Carlo Morabito. A time-frequency based machine learning system for brain states classification via eeg signal processing. In *2019 International Joint Conference on Neural Networks (IJCNN)*, pages 1–8. IEEE, 2019.

SUPPLEMENTARY MATERIAL

S.I. DATA AUGMENTATION BANKS

Temporal Flipping. We reverse the EEG data along the temporal dimension. The probability to apply is controlled by a parameter *prob*, with a default value of 0.5.

Temporal Masking. We randomly mask timestamps across all channels. The proportion of timestamps masked is controlled by the parameter *ratio*, with a default value of 0.1.

Frequency Masking. We convert the EEG data into the frequency domain, randomly mask some frequency bands, and convert it back. The proportion of frequency bands masked is controlled by the parameter *ratio*, with a default value of 0.1.

Channel Masking. We randomly mask channels across all timestamps. The proportion of channel masked is controlled by the parameter *ratio*, with a default value of 0.1.

Jittering. Random noise, ranging from 0 to 1, is added to the raw data. The intensity of the noise is adjusted by the parameter *scale*, which is set by default to 0.1.

Dropout. Similar to the dropout layer in neural networks, this method randomly drops some values. The proportion of values dropped is controlled by the parameter *ratio*, with a default value of 0.1.

S.II. DATASETS

ADFTD. The ADFTD-RS (A dataset of EEG recordings from Alzheimer’s disease, Frontotemporal dementia and Healthy subjects) is a publicly available resting-state EEG dataset on the OpenNEURO website⁵ from the paper [22], [62], and a complementary dataset ADFTD-PS(A complementary dataset of open-eyes EEG recordings in a photo-stimulation setting from: Alzheimer’s disease, Frontotemporal dementia and Healthy subjects) in a photo-stimulation setting with exactly matched subjects⁶. It contains 88 subjects, including 36 AD, 23 Frontotemporal Dementia (FTD), and 29 healthy controls. We preprocess the two sub-datasets, ADFTD-RS and ADFTD-PS, and concatenate them by subject ID.

CNBPm. The CNBPM [63], [73] is a large private EEG dataset provided by the AI-LAB laboratory at the University Mediterranea of Reggio Calabria, Italy. It consists of 63 subjects with Alzheimer’s Disease (AD), 63 with Mild Cognitive Impairment (MCI), and 63 Healthy Control (HC) subjects. The data are collected using 19 channels international 10-20 system with an initial sampling rate of 1024Hz.

P-ADIC. The P-ADIC⁷ dataset, introduced in [64] and publicly available via DRYAD, includes EEG recordings from 249 subjects (although the original paper reports 230). The dataset includes 49 individuals with Alzheimer’s Disease (AD), 34 with Mild Cognitive Impairment (MCI), 96 Healthy Controls (HC), 42 with Schizophrenia, and 28 with Depression.

CAUEEG. The CAUEEG⁸ dataset, introduced in [53], is available upon request and contains 1,379 EEG recordings from

⁵<https://openneuro.org/datasets/ds004504/versions/1.0.8>

⁶<https://openneuro.org/datasets/ds006036/versions/1.0.5>

⁷<https://datadryad.org/dataset/doi:10.5061/dryad.8gtht76pw>

⁸<https://github.com/ipsis-mjkim/caueeg-dataset>

1,155 subjects. It includes 459 recordings from healthy controls (HC), 417 from individuals with Mild Cognitive Impairment (MCI), 311 with dementia, and 192 with other conditions. In line with the protocol described in their paper, we treat each EEG recording as an independent subject. This decision is based on reported label shifts across sessions (e.g., HC to MCI, MCI to AD), suggesting that different recordings from the same individual should be considered distinct.

S.III. IMPLEMENTATION DETAILS

Manual Feature utilize 32 features, including mean, variance, skewness, kurtosis, std, iqr, max, min, mean, median, delta power, theta power, alpha power, beta power, total power, theta alpha ratio, alpha beta ratio, delta relative power, theta relative power, alpha relative power, beta relative power, phase coherence, spectral centroid, spectral rolloff, spectral peak, average magnitude, median frequency, amplitude modulation, spectral entropy, tsallis entropy, and shannon entropy. A linear layer is then applied to perform final classification.

EEGNet [66] is a classic deep learning method for EEGNet decoding. It uses depthwise and separable convolutions to capture spatial and temporal features. We keep the same structure and order when applying convolutions, normalization, and activations as described in the paper.

TST [67] is introduced to apply the transformer to time series data. It embeds each cross-channel timestamp as an input token for self-attention. We set *e_layers* = 12, *n_heads* = 8, *d_model* = 128, and *d_ff* = 256.

EEGInception [68] uses different scales of convolutional kernels, combined with a spatial block for feature extraction. We set *n_blocks* = 3, *channels* = (96,192,384), *kernel_sizes* = (8,16,32), *depth_multiplier* = 2, *bottleneck_channels* = 32.

EEGConformer [47] uses convolutional modules to learn low-level local features and embed the raw data into patches for self-attention. We set *e_layers* = 12, *n_heads* = 8, *d_model* = 128, and *d_ff* = 256.

BIOT [48] employs single-channel patch embedding to handle biosignals with varying numbers of channels. Each patch is mapped into tokens, with segment embedding, channel embedding, and positional embedding added to make the tokens distinguishable. We set *e_layers* = 12, *n_heads* = 8, *d_model* = 128, and *d_ff* = 256.

MedGNN [69] is a graph-nerual-network-based method for medical time-series classification. It uses a multi-resolution graph transformer architecture to model the dynamic dependencies and fuse the information from different resolutions. We set *-resolution_list* = 2,4,6,8, *-nodedim* = 10, *e_layers* = 12, *n_heads* = 8, *d_model* = 128, and *d_ff* = 256.

Medformer [32] is designed for biomedical time series classification, including EEG and ECG. Cross-channel multi-granularity patch embedding and intra-inter-granularity self-attention are utilized. We extended our work based on this method. We set *e_layers* = 12, *d_model* = 128, and *d_ff* = 256, *patch_len_list* = [2, 4, 8].

ADformer The detailed parameters of our method are provided in script files in the GitHub repository with link <https://github.com/DL4mHealth/ADformer>.